

Parallel single molecule detection with a fully integrated single-photon 2×2 CMOS detector array

Michael Gösch

Karolinska Institute
Department of Medical Biochemistry and Biophysics
S-171 77 Stockholm, Sweden
and
École Polytechnique Fédérale de Lausanne
Laboratoire d'Optique Biomedicale
CH-1015 Lausanne, Switzerland

Alexandre Serov

Tiemo Anhut

Theo Lasser

École Polytechnique Fédérale de Lausanne
Laboratoire d'Optique Biomedicale
CH-1015 Lausanne, Switzerland

Alexis Rochas

Pierre-André Besse

Radivoje S. Popovic

École Polytechnique Fédérale de Lausanne
Institute of Microelectronics and Microsystems
CH-1015 Lausanne, Switzerland

Hans Blom

Royal Institute of Technology
Department of Microelectronics and Information
Technology
Electrum 229
S-16440 Kista, Sweden

Rudolf Rigler

Karolinska Institute
Department of Medical Biochemistry and Biophysics
SE-171 77 Stockholm, Sweden
E-mail: rudolf.rigler@mbb.ki.se

1 Introduction

Confocal spectroscopy in combination with fluorescence correlation spectroscopy (FCS) is an experimental technique used for examination of the chemical and photophysical dynamics at the single-molecule level (see the review in Ref. 1). Here, an autocorrelation curve is obtained by measuring the random intensity fluctuations of a fluorescent signal generated by the radiative relaxation of light-excited molecules.^{2–4} A remarkable SNR is achieved by inserting a pinhole, thereby generating a confocal detection volume of femtoliter order.⁵ Recently, FCS has emerged as a powerful method for analyzing dynamic processes at the molecular level: molecular interactions,^{2,3} conformational changes,^{6,7} chemical reactions,⁸ protein binding to cell membranes,⁹ photophysical dynamics,¹⁰ and transport or flow properties¹¹ are examples of subjects examined by FCS. In addition, FCS can also be a powerful tool for drug discovery and development and diagnostic tests in medicine.^{1,12,13}

Address all correspondence to Rudolf Rigler, Karolinska Institute, Department of Medical Biochemistry and Biophysics, SE-171 77 Stockholm, Sweden. Tel: +41-21-693-8700; Fax: +41-21-693-8700; E-mail: rudolf.rigler@mbb.ki.se

Abstract. We present parallel single molecule detection (SMD) and fluorescence correlation spectroscopy (FCS) experiments with a fully integrated complementary metal oxide semiconductor (CMOS) single-photon 2×2 detector array. Multifocal excitation is achieved with a diffractive optical element (DOE). Special emphasis is placed on parallelization of the total system. The performance of the novel single-photon CMOS detector is investigated and compared to a state-of-the-art single-photon detecting module [having an actively quenched avalanche photodiode (APD)] by measurements on free diffusing molecules at different concentrations. Despite the order of magnitude lower detection efficiency of the CMOS detector compared to the state-of-the-art single-photon detecting module, we achieve single molecule sensitivity and reliably determine molecule concentrations. In addition, the CMOS detector performance for the determination of the fraction of slowly diffusing molecules in a primer solution (two-component analysis) is demonstrated. The potential of this new technique for high-throughput confocal-detection-based systems is discussed. © 2004 Society of Photo-Optical Instrumentation Engineers. [DOI: 10.1117/1.1781668]

Keywords: parallel single molecule detection; single-photon detector; complementary metal oxide semiconductor technology; detector arrays; parallel confocal spectroscopy; fluorescence correlation spectroscopy.

Paper 03104 received Aug. 11, 2003; revised manuscript received Jan. 27, 2004; accepted for publication Feb. 17, 2004.

Further development of FCS requires the design of new devices, e.g., detectors in our case, with improved performance, extended capacities, and reliable throughput features. One of the rapidly developing markets where this technique is used is biochip microarray analysis. Today's microarray systems feature from a few up to a hundred thousand^{13–15} sampled spots on a single biochip. Therefore, a high-spatial-resolution technique is required for both the fabrication process and detection. The measurement time for scanning a microarray with confocal FCS is directly proportional to the number of measured spots and often can reach a few hours. The use of intensified CCDs, with several thousand detector elements, is not a solution for parallel FCS detection of single molecules, as CCD-based systems have a much longer read-out time compared to the 1-ns to 1-ms dynamics of single-photon events (although single-photon sensitivity can be achieved with a cooled system). To increase the detection speed it is necessary to achieve multiplexing (parallelism) with high spatial resolution. Obviously, a parallel detection approach will enable enhanced analysis speed as compared to a single confocal laser focus. This would extend the range of

applications of FCS, particularly for use with high-density microarrays and for the detection of molecules at very low (picomolar) concentrations.

Recently, a first spatial multiplexing experiment at the single-molecule level was reported by Blom et al.^{14,16} Multifocal excitation with a 2×2 fan-out diffractive optical element (DOE), resulting in four confocal volume elements, was performed. The detection of the fluorescence signal was realized through four optical fibers coupled to commercially available single-photon detection modules. The feasibility of the parallel approach was demonstrated by measurements on dye labeled nucleotides. However, the use of fiber optics is limited to a small number of parallel channels, because otherwise the detection stage adjustment would become unmanageably complex.

In this paper, we report confocal detection experiments utilizing a fully integrated 2×2 array of Geiger-mode avalanche photodiodes made by an industrial complimentary metal-oxide semiconductor (CMOS) process, which we will henceforth refer to as the CMOS single-photon avalanche detector (CMOS SPAD). Single pixels as well as detector arrays integrated with the driving electronics were optically characterized by Rochas et al.^{17,18} Despite the low detection efficiency of the CMOS SPAD we nonetheless demonstrate, with an array of such detectors, the feasibility of a parallel FCS single molecule detection approach and compare the performance of our new detector to that of a commercially available high-performance single-photon counting module from Perkin Elmer Optoelectronics (the SPCM-AQR-13, a specific avalanche photodiode actively quenched by a hybrid electronics). Comparative analysis of parameters such as dead time, dark count rate, afterpulsing, and detection efficiency were performed. The influence of the measurement time on precision of fitting parameters associated with the FCS correlation function is also evaluated. Finally, we demonstrate the application of our new single-photon detector array for multispot FCS experiments.

2 Theory

The basics of FCS were established around 25 years ago.^{2-4,19} Detailed reviews on FCS can be found elsewhere.^{1,12,20} In general, excitation laser light is focused into a sample, usually a droplet or, as used in high-throughput screening, into different spots corresponding to microarray wells. Every molecule diffusing through the excitation focus gives rise to fluorescence photon bursts. The length of each photon burst corresponds to the time the molecule spends in the detection volume element. To reject stray light and thereby increase the SNR, the excitation focus is imaged onto a pinhole.⁵ Subsequently, the fluorescence emission photons are focused onto the active area of an avalanche photodiode (APD) or another single-photon detector working in the Geiger mode [e.g., a photomultiplier tube (PMT), CMOS SPAD]. Every detected fluorescence photon generates a pulse that is sent to a correlator, where the autocorrelation function of the fluorescence intensity fluctuations is calculated.

The autocorrelation curve contains information about the dynamics of intensity fluctuations in the time interval from 30 ns (the dead time of the detector) to the length of the measurement. The basic parameters that can be achieved by fitting

the autocorrelation function with an analytical expression are diffusion time (mean residence time of a molecule in the detection volume element), average number of molecules in the detection volume element, molecule fractions (if several types of different diffusing molecules are present in the sample), and the fraction of particles occupying the triplet state (longer lifetime nonfluorescent dark states).

For the simplest possible case of diffusion of a single chemical species in a dilute solution the analytical expression of the autocorrelation function is⁵

$$G(\tau) = \frac{\langle I(t+\tau)I(t) \rangle}{\langle I(t) \rangle^2} = 1 + \frac{1}{N} \left(1 + \frac{\tau}{\tau_D} \right)^{-1} \left(1 + \frac{\tau}{R^2 \tau_D} \right)^{-1/2}, \quad (1)$$

where $I(t)$ is the intensity of the fluorescence present in the detection volume element; $\langle \rangle$ denotes the time average; N is the average number of molecules present in the detection volume element ($V = \pi^{3/2} \omega_{xy}^2 \omega_z$); $R = \omega_z / \omega_{xy}$ is the ratio of the axial (w_z) to the radial (w_{xy}) dimensions of the confocal detection volume element; and $\tau_D = \omega_{xy}^2 / 4D$ denotes the radial diffusion time through the illumination region, where D is the diffusion coefficient. Thus, the average concentration of the molecules in the volume element can be found as $C = N/V$.

The analytical expression for a multiple number of chemical species having differing molecular weights and moving freely and independent can be written as²¹

$$G(\tau) = 1 + \frac{\sum (N_j/N_1)(v_j/v_1)^2 (1 + \tau/\tau_{Dj})^{-1} [1 + \tau/(R^2 \tau_{Dj})]^{-1/2}}{N_1 [\sum (N_j/N_1)(v_j/v_1)]^2}. \quad (2)$$

Here, contributions of each different molecular species (denoted by the index j) present in the detection volume element are weighted with the specific count rate per molecule, v_j . In the present case, only a two-component solution [slower (primer) and faster (dye) diffusing molecules] are considered.

The total count rate I can be expressed as

$$I = (N_1 v_1) \sum \frac{N_j v_j}{N_1 v_1}, \quad (3)$$

whereby this representation of I becomes evident, when introducing the ratio $q = v_j/v_1$ [see also Eq. (5)].

3 Experiments

3.1 Setup

The experimental configuration for parallel excitation and detection is displayed in Fig. 1 (a single-point measurement is realized without the DOE in the illumination part). The laser beam from a diode-pumped solid state laser (532 nm, Kimmon DPSS Laser, model-5526) was enlarged by a beam expander [$L_1(f=25 \text{ mm}), L_2(f=400 \text{ mm})$] to fully illuminate the diffractive optical element (for details on DOEs see Ref. 22) and to overfill the back aperture of the microscope objective. Using the collimating lenses [$L_3(f=150 \text{ mm}), L_4(f=150 \text{ mm})$], the DOE, and the microscope objective, the ex-

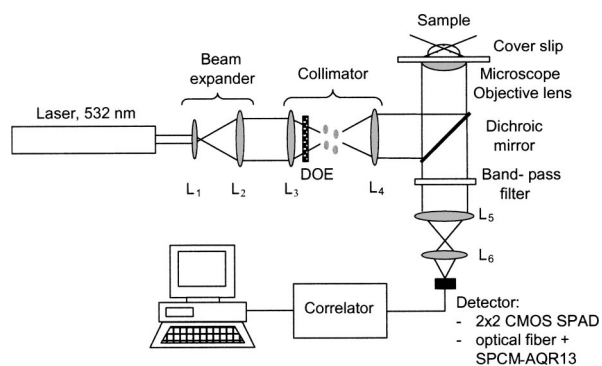


Fig. 1 Experimental configuration for parallel FCS measurements.

panded beam was reshaped into a 2×2 -foci pattern and focused into the sample. The intensity in a single spot was measured to be 1.7 mW at the entrance of the objective. The excitation light was reflected by a dichroic mirror (Chroma, 565LP) into a $40\times$ numerical aperture (NA) 1.15 water immersion objective (Olympus, Uapo/340, cover slip corrected). The fluorescence emission was collected by the same objective and transmitted through a bandpass filter (Chroma HQ585/40) that discriminated the signal from Rayleigh- and Raman-scattered light. Finally, the fluorescence emission was focused by the tube lens [L_5 ($f = 180$ mm)] and a $4\times$ demagnifying lens [L_6 ($f = 35$ mm)] onto either one detector (\varnothing 7 to $8 \mu\text{m}$, see Fig. 2) of the 2×2 CMOS SPAD array or onto the optical fiber (\varnothing $9 \mu\text{m}$) connected to the SPCM-AQR-13. An XYZ translation stage holding the 2×2 CMOS SPAD array or the fiber connected to the SPCM-AQR-13 enabled spatial fine adjustment of the detector(s). The photoinduced pulses from the detectors were registered by a hardware correlator (Correlator.com, Flex990EM-12C), which calculated the autocorrelation function. The calculated functions were stored in computer memory and then analyzed with an in-house computer program based on the Marquardt-Levenberg nonlinear least-squares minimization algorithm weighted after Koppel²³ that produces the number of molecules and the molecular diffusion times as fitting parameters.

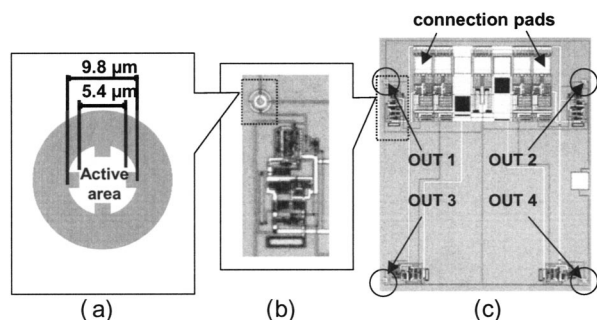


Fig. 2 (a) Geometrical configuration of a single CMOS SPAD, where the effective diameter of the sensitive area corresponds to 7 to $8 \mu\text{m}$; (b) single CMOS SPAD with integrated electronics; and (c) chip having a 2×2 CMOS SPAD array: OUT 1 to OUT 4 show the positions of the active areas; the distance between each is 1.1 mm.

3.2 Single-Photon Detectors

APDs and PMTs are presently used for measuring fluorescence signals in FCS experiments. The detection efficiency of APDs (typically 70%) is higher than that of PMTs (around 10%). APDs have a higher dark count rate (250 to 500 Hz versus 15 Hz for PMTs), a higher afterpulsing probability (1 to 3% versus 0.1% for PMTs) and a longer dead time (50 versus 25 ns for PMTs). All of these parameters (dead time, afterpulsing, detection efficiency, and dark count) cause artifacts influencing the accuracy and/or precision of FCS measurements. Dead time and afterpulsing limit the shortest time lag accessible in a photon correlation experiment and also introduce correlated signal contribution to the modeled auto-correlation curve. Detection efficiency and dark counts influence the SNR of the measurement. Due to technological limitations, APDs and PMTs alike cannot be used directly in multispot FCS systems incorporating large numbers of spots. These detectors are not compatible with integration of processing electronics and the photodetector on the same chip. However, CMOS technology enables the design of photodetector arrays and the simultaneous integration of necessary electronics onto a single chip. Recently, the first array of Geiger APDs made by an industrial CMOS process (CMOS SPAD) was designed and successfully tested in the Microsystems Laboratory of the Swiss Federal Institute of Technology, Lausanne¹⁸ (Switzerland). A similar CMOS SPAD detector and its performance in FCS measurements is described in this paper.

3.3 Beam Quality on the Detector

Our experimental configuration shows off-axis aberrations (mainly coma and astigmatism) due to the fact that the DOE generates the confocal spots beside the optical axis. Since the microscope system itself is aberration corrected, the strongest aberrations are expected from the demagnifying lens (L_6) placed in the detection arm of the system. The small size of the active area of the CMOS detectors makes the detection system sensitive to the contribution of aberrations, merely affecting the total collection efficiency. Our simulations utilizing ZEMAX (Focus Software, Inc.) showed that for a 2×2 -foci system, we could expect a decrease in the collection efficiency of a factor 2 to 5 in comparison to an on-axis single-point illumination scheme.

3.4 Samples

A nucleotide triphosphate (tetramethylrhodamine-6-dCTP, New England Labs-425) henceforth referred to as TMR, diluted from a stock solutions ($1 \mu\text{M}$) in Millipore water to concentrations of 0.5, 2.5, and 1 nM, was used for single-component diffusion measurements.

For two-component diffusion measurements, the binding of different biological molecules to each other can be detected with FCS only when the difference in diffusion time is sufficiently high.^{24,25} Therefore, an high-performance liquid chromatograph (HPLC) pure primer template with 42 nucleotides (CTCGGGCTAAGGAGATTGTGTGGAATGGTCTGTGGGGGTAT, Thermo Hybaid, Ulm, Germany) tagged on the 5'-end with a TAMRA dye was chosen. The molecular weight given is $M_{\text{primer}} = 13,822$ g/mol and $M_{\text{free_dye}} \approx 500$ g/mol. A 10-nM primer concentration was mixed with a 10-nM dye

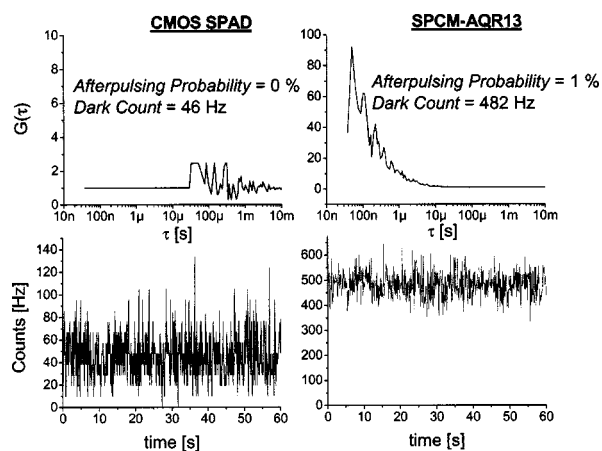


Fig. 3 Measured autocorrelation curves and trace signals of dark counts obtained from the CMOS SPAD and the SPCM-AQR-13 for a 60-s measurement.

concentration in different ratios (between 10/0 and 1/9) and each mixture was measured with the two detectors, CMOS SPAD and SPCM-AQR-13, in triplicates.

4 Measurements and Results

4.1 CMOS SPAD versus SPCM-AQR13: Dead Time, Afterpulsing, Dark Counts, and Detection Efficiency

In this subsection we compare the performance of the CMOS SPAD with the SPCM-AQR-13 commercial single-photon counting module normally used in FCS experiments.

Figure 3 shows autocorrelation curves (averaging time is 60 s) and trace signals of dark counts measured with our CMOS SPAD [OUT 1, see Fig. 2(c)] and the SPCM-AQR-13. As we can see from the figure, our detector does not have any measurable afterpulsing effect. The SPCM-AQR-13 module shows an afterpulsing signal expanding up to $\tau = 10 \mu\text{s}$ in the correlation curve. For dynamical processes in the microsecond range (e.g., triplet states), this afterpulsing could bias the result significantly. The corresponding signal traces, shown in the bottom plots, demonstrate the dark count level for both photodetectors, which is about 50 Hz for the CMOS SPAD and around 500 Hz for the SPCM-AQR13.

Figure 4 demonstrates typical autocorrelation function curves (averaging time is 60 s) of freely diffusing TMR nucleotide measured with our CMOS SPAD and the SPCM-AQR13. The dye-labeled molecules were dispersed in a droplet on a cover glass at a concentration of 2.5 nM. The autocorrelation curves are distorted differently by the effects of dead time and afterpulsing. The CMOS SPAD exhibits only a small distortion due to dead time, which is not higher than 30 ns, visible as a gap at lower values of τ . For the SPCM-AQR13 module, one can see distortions caused by afterpulsing, the sharp peak at 100 ns, as well as the dead time, which is estimated to be approximately 50 ns.

The analytical autocorrelation function [Eq. (1)] was fitted to the obtained data. The autocorrelation function for $\tau < 10 \mu\text{s}$ was not taken into account to exclude the triplet state and afterpulsing effects for the SPCM-AQR13. From the fits, the average number of molecules per volume element is N

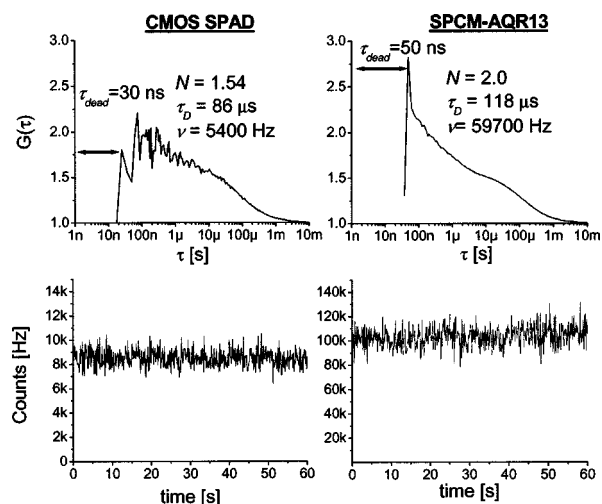


Fig. 4 Typical autocorrelation curves and trace signals of TMR solution (2.5 nM) measured with the CMOS SPAD and the SPCM-AQR-13 for 60 s.

$= 1.54$ for the CMOS SPAD and $N = 2.0$ for the SPCM-AQR13. The radial diffusion times are $\tau_D = 86$ and $118 \mu\text{s}$, respectively. These differences are caused by the fact that the measured confocal volumes V for the SPCM-AQR-13 coupled to a $9\text{-}\mu\text{m}$ optical fiber and our detector, which has an effective diameter of 7 to $8 \mu\text{m}$ (see Fig. 2), are slightly different. In addition, the afterpulsing probability of the SPCM-AQR-13 is also higher. Therefore, a systematic error can be introduced by the measurement as well.

In Fig. 4, the count traces of the measured fluorescence signal demonstrate the sensitivity of the two systems. As one can see from the traces, the sensitivity of the CMOS SPAD is about one order of magnitude lower than that of the SPCM-AQR13. The efficiency of the SPCM-AQR13 is given in the technical specifications to be around 70%, which provided a count rate of $\nu = 59700 \text{ Hz}$ in the experiment. The CMOS SPAD has only 6 to 7% detection efficiency, which resulted in $\nu = 5400 \text{ Hz}$. Table 1 lists the characteristics of the two investigated detectors.

4.2 CMOS APD versus SPCM-AQR13 Module: Fitting Error versus Sampling Time for Measurements on the Single-Molecule Level

In the following experiment we measured the influence of the averaging time on the statistical reliability of an FCS measurement. The statistical reliability of the FCS measurements for the two detectors was tested with diffusing-dye-labeled nucleotides. The number of molecules in the sample volume

Table 1 Performance characteristics of the two detection systems.

Detector System	Detection Efficiency at $\lambda = 565 \text{ nm}$	Dark Count Rate (Hz)	Afterpulsing Probability (%)	Dead Time (ns)
SPCM-AQR13	60–70%	500	1	50
CMOS SPAD	6–7%	50	0	30

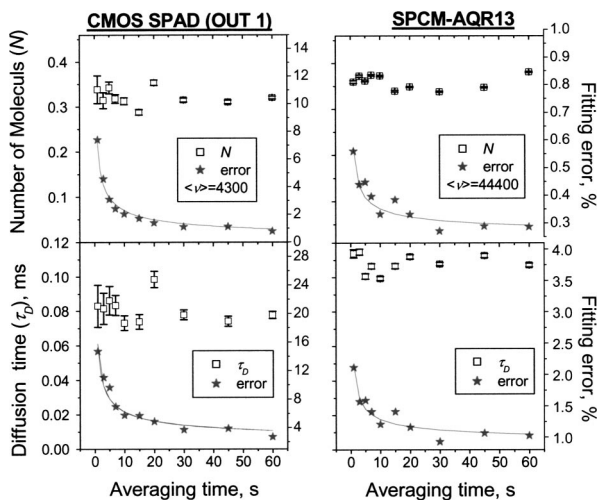


Fig. 5 Left Y axes: measured number of molecules (N) in the sampling volume and diffusion time (τ_D) as functions of the averaging time; right Y axes: fitting error (standard error in fitting coefficient). Measurements were performed with the CMOS SPAD and a commercial single-photon counting module (SPCM-AQR-13) at TMR at a 500-pM concentration. The solid line is a fit of the error data points with the equation $y = a + b/\sqrt{T}$; see text for details.

never exceeded 1, which means that on average at the most one molecule was present in the detection volume.

For most biological applications, the concentration of fluorescent molecules in the sample is important to know. With FCS the average concentration of fluorescent molecules ($C \propto N$) and the diffusion time (τ_D) can be obtained by fitting the measured correlation curve with the described analytical autocorrelation function [see Eq. (1) or (2)]. The number of photons per molecule detected within a certain time interval influences the FCS statistical reliability, or the “smoothness,” of the correlation function, and thus decreases the standard deviation, which, in turn, finally influences the precision of the estimated values of τ_D and N .

Measurements were performed with the CMOS SPAD and the SPCM-AQR-13 detector on two different concentrations of TMR molecules (2.5 nM and 500 pM). The measurements on the 500-pM solution are displayed in Fig. 5, which shows the measured number of molecules in the detection volume element and the diffusion time as functions of the acquisition time (averaging time) chosen to be 1, 3, 5, 7, 10, 15, 20, 30, 45, and 60 s. The dependence of the fitting error (standard deviation in fitting coefficient) on the acquisition time is shown on the right Y axis for each graph.

The measurements performed with the SPCM-AQR13 gave a better statistical reliability and consequently a smaller fitting error; the latter of is always less than 0.6% for N and 2.5% for τ_D . The maximal fitting errors obtained with the CMOS SPAD are 8 and 16%, respectively (see Fig. 5). However, for longer averaging times, the fitting error is strongly reduced, and even in the sub-single-molecule measurement regime ($N < 1$) our detector showed a good statistical reliability with fitting errors smaller than 1.2% for N and smaller than 5% for τ_D for a 20-s acquisition time. The different statistical accuracies that we obtained with the two detectors are ex-

plained by the SNR for FCS measurements, which is given by^{23,26,27}

$$\text{SNR} = \frac{G(\tau)}{\{\text{var}[G(\tau)]\}^{1/2}} \approx \nu\sqrt{T}. \quad (4)$$

Here, ν is the count rate per molecule, and T is the acquisition time. In consequence of Eq. (4), the SNR depends more strongly on ν than it depends on T . This means a 10-fold loss of detection efficiency must be compensated for by a 100-fold increase in acquisition time to achieve the same SNR.

In our measurements, the error data points (“stars” in Fig. 5) were fitted with $y = a + b/\sqrt{T}$, in accordance with Eq. (4). Here, the parameter a is due to a systematic error of the measurements. The parameter b is inversely proportional to the count rate (ν) and had an approximately order of magnitude higher value for the CMOS SPAD than for the SPCM APD, a difference clearly resulting from the lower detection efficiency of the CMOS SPAD. However, the measurements performed with the CMOS SPAD at a 500-pM concentration gave results with an error rate of <5% after only 5 s for the determination of the number of molecules N and after 15 s for the diffusion time τ_D . For applications where the relative difference in number of molecules or diffusion time is decisive, such an error might be acceptable.

4.3 Biologically Relevant Two-Component Analysis with CMOS SPAD

The two-component analysis is interesting for many different biological applications. This analysis method has been applied previously to investigate the hybridization of DNA strands to each other and to RNA and the binding of ligands to their receptors and to other proteins.^{1,28} We investigated if molecules having different diffusion times could be identified equally well with both detectors: the CMOS SPAD and the SPCM-AQR-13. The 10-nM primer concentration was mixed with a 10-nM dye concentration in different ratios between 10/0 and 1/9 and measured with the two detectors in triplicate. The autocorrelation curves of the measured samples were fitted in the time interval from approximately 10 μ s to 30 s. The autocorrelation signal at times less than 10 μ s was excluded to diminish the effect of afterpulsing (which is only present in the SPCM-AQR-13 detected autocorrelations) as well as to exclude the contribution of the triplet states. To evaluate the performance of the two detectors, the percentage of molecules with the slower diffusion component (primer) in relation to the more rapidly diffusing molecules (dyes) was determined as follows:

First, the autocorrelation curve obtained on a pure dye solution was analyzed with Eqs. (1) and (3) to estimate the ratio of the axial and radial dimensions $R = \omega_z/\omega_{xy}$, the diffusion time (τ_{D1}), and the count rate per molecule (ν_1) of the free dye. The values were determined to be $R = 8$, $\tau_{D1} = \tau = 100 \mu$ s, and $\nu_1 = 3900$ Hz for the CMOS SPAD and $R = 9$, $\tau_{D1} = \tau = 110 \mu$ s, and $\nu_1 = 48,600$ Hz for the SPCM-AQR-13.

Second, the purity of the HPLC pure primer was determined by an HPLC (Spectra Systems, ThermoFinnigan with Vydac 214TP reverse phase column, Dionex). Here, free TAMRA dyes could still be identified in the sample. Therefore, the count rate per molecule of the primer ν_2 , could not

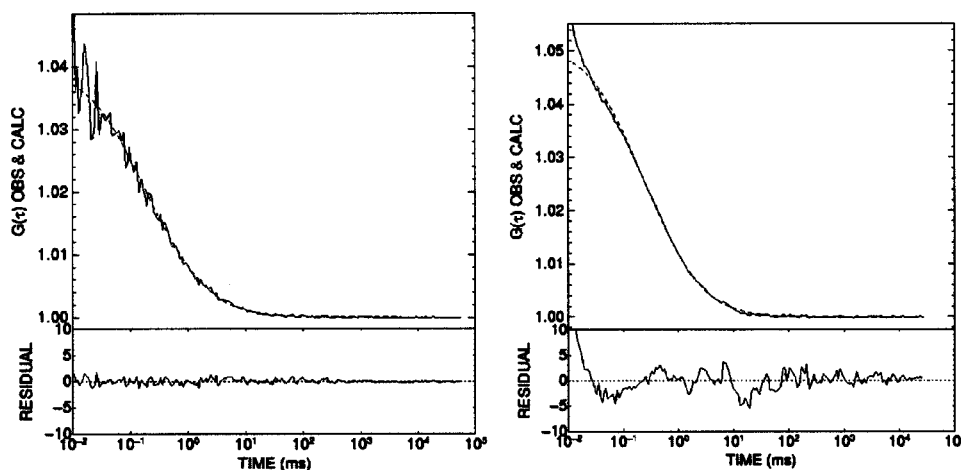


Fig. 6 Measured two-component diffusion autocorrelation curves obtained with the CMOS SPAD (left), the mean count rate was around $I = 30$ kHz, $N_1 = 5.2$, and $N_2 = 30.6$, and SPCM-AQR-13 (right), the mean count rate was around $I = 380$ kHz, $N_1 = 2.8$, and $N_2 = 23.3$. The primer fraction (more slowly diffusing component) was in both cases determined to be around $PF = 85\%$. The dotted lines in both plots show the curve fitted to the experimental data. Due to the lower detection efficiency of the CMOS SPAD detector, the noise in the autocorrelation function is worse than for the SPCM-AQR-13. However, the residuals of the CMOS SPAD, with no afterpulsing, show lower and more consistently varying values than for the SPCM-AQR-13.

be measured experimentally. Instead, we estimated the count rate per molecule of the HPLC pure primer to be one third of the count rate per molecule of the free dye ν_1 . Following Eq. (2) we get

$$G(\tau) = 1 + \frac{(1 + \tau/\tau_D)^{-1} [1 + \tau/(R^2\tau_{D1})]^{-1/2}}{N_1(1 + qn)^2} + \frac{q^2n(1 + \tau/\tau_{D2})^{-1} [1 + \tau/(R^2\tau_{D2})]^{-1/2}}{N_1(1 + qn)^2}. \quad (5)$$

Here, $q = \nu_2/\nu_1$ and $n = N_2/N_1$; and ν_1 and ν_2 are the count rate per molecule and N_1 and N_2 are the number of molecules in the confocal volume for the free dye and for the primer, respectively.

Third, the recorded autocorrelation curves of the different primer-dye mixtures from both detectors were analyzed (see Fig. 6) with the described in-house fitting program. Here, the ratio of the axial and radial dimensions of the detection volume element (R), the diffusion time of the free dye (τ_{D1}), and the coefficient $q = 0.3$ were fixed. The fitting of Eq. (5) gave the diffusion time of the primer ($\tau_{D2} = 0.7$ and $\tau_{D2} = 0.6$ for the CMOS SPAD and the SPCM APD, respectively), the coefficients n , and the number of molecules N_1 . Finally, the primer fraction was determined as $PF = N_2/(N_1 + N_2)$. Figure 7 shows this ratio with reference to the theoretically calculated fraction of the primer (from the mixing of the two components).

It turned out that the estimated ratio of the count rates per molecule $q = 0.3$ was not exactly correct. In consideration of Eq. (3) (where I is the mean count rate obtained in one measurement), the ratio of the count rates per molecule was probably even lower. The reason for this increment count rate lies in the oversimplification of the biological compound model. Here, obviously, more than two compounds with different count rates per molecule ν were present in the sample (e.g.,

free dyes, dye-labeled primer, and primer with intercalated dyes) making the determination of the exact absolute values of N_1 and N_2 difficult. However, the relative values based on measurements with the CMOS SPAD are quite similar compared to the relative values obtained by the measurements with the SPCM-APD. Thus, both detectors can be used for, for instance, concentration determinations of unknown mixtures giving a calibration curve, as in Fig. 7. The experimentally obtained primer fractions do not differ systematically, but only stochastically, between the two different detectors, the CMOS SPAD and the SPCM-AQR-13. Despite the fact that the detection efficiency of the CMOS SPAD is approximately 10 times lower than that of the SPCM-AQR-13, the measurement time for the CMOS SPAD was only two times longer and very similar results are found for both detectors. In conclusion, the CMOS detector as well as the commercially

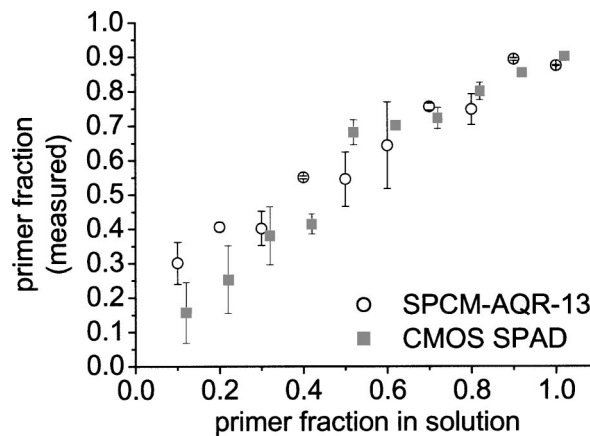


Fig. 7 Experimentally measured fraction of primer molecules (PF) as a function of the estimated primer fraction in solution (determined by the volumetric ratio of the primer and dye solutions).

available high-performance single-photon detector (as APD) can be used in FCS.

Ten samples with different primer concentrations were measured for 60 s each and the resulting autocorrelation curves were analyzed (see Fig. 7). Even in the HPLC pure primer solution approximately 10% of free dyes were found. Therefore, the highest value of the measured primer fraction resulted only in approximately 90%. Independent measurement by HPLC confirmed the existence of free dye molecules also (data not shown). Each data point in Fig. 7 is the average of the three values from the three independent measurements. The error bars indicate the standard deviation for the measurement point. An offset on the abscissa of 0.02 has been introduced for the CMOS SPAD to avoid an overlap of the data points in the graph.

4.4 Parallel Single-Molecule Detection and Parallel FCS with 2×2 CMOS SPAD Array

In this section the results obtained with the multifocal diffractive optical FCS system are presented. Also here, the concentration of molecules was so low that single-molecule detection could be performed. We utilized one of our 2×2 CMOS SPAD arrays to demonstrate its potential for parallel FCS experiments. Since the manufacturing process is not yet optimized for the homogeneous performance of all four detectors,¹⁸ we chose one of the arrays that has pixels with essentially different dark count rates: 40, 30, 400, and 2000 Hz for OUT1 to OUT4 [Fig. 2(c)], respectively. With this detector, the impact of the nonuniformity of the detector parameters to the measurement accuracy was estimated.

A 1-nM solution of TMR was dispersed in a droplet on a cover glass. The 2×2 fan-out diffractive optical foci were then positioned into four arbitrary points of the drop. The measurement time was 300 s. Figure 8 illustrates the result of the measurements performed with the 2×2 FCS system on a 1-nM TMR sample. The first three detectors show a similar performance: the average number of molecules $\langle N \rangle = 0.88 \pm 0.04$, the average diffusion time $\langle \tau_D \rangle = 88 \pm 8 \mu\text{s}$, and the average count rate per molecule $\langle \nu \rangle = 2000 \pm 280 \text{ Hz}$. The relative differences can be explained by the individual response of the four detectors as well as the positioning inaccuracy of the conjugated confocal spots on the detectors. Similar differences (<20%) also can be observed in single-spot FCS measurements. The fourth detector has a higher dark count rate (2000 Hz) but the same detection efficiency. This results in a flattening of the autocorrelation trace and the fitting of the curve has to be corrected for this background signal.²⁹ Even with such a correction we get higher values for $N = 2.6$, $\tau_D = 166 \mu\text{s}$ and an almost fourfold lower ν value (590 Hz). One explanation for these differences could be that aberration occurred, which results in different confocal spots. Another would be that the DOE was somehow tilted and the distance between the spots was no longer optimized toward the distance between the active pixels of the detector array. Thereby, the excitation volume elements did not coincide 100% with the active areas of the CMOS SPAD array, which resulted in a larger confocal volume per spot as well as in lower collection efficiency for the different foci. Finally, we calibrated the confocal volume for each sensor on the basis of the radial diffusion times. With an estimated diffusion coefficient^{5,14} of D

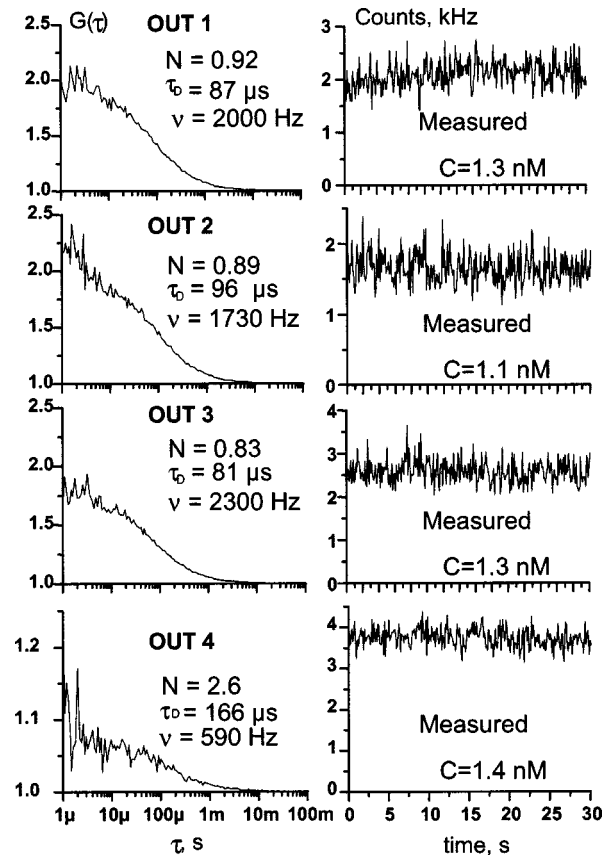


Fig. 8 Autocorrelation functions (left) of fluorescence signals (right) measured in a solution of 1-nM dye-labeled nucleotide triphosphates (TMR) from four DOE-generated foci with a 2×2 CMOS SPAD array.

$= (kT)/(6\pi\eta r) = 2.6 \times 10^{-10} \text{ m}^2/\text{s}$, and using $V = R(4\pi\tau_D D)^{3/2}$, we estimated the detection volume elements for each of the four detectors to be 1.2, 1.4, 1.1, and 3.2 fl, respectively. From these values, the concentration values were determined to be 1.3, 1.1, 1.3, and 1.4 nM, respectively. This calibration method ensures that all detectors give a similar quantitative measure. This result demonstrates the feasibility of our parallel FCS system in the sub-single-molecule ($N < 1$) range.

5 Conclusion

We presented parallel FCS measurements with a 2×2 Geiger-mode single-photon APD array made in a conventional CMOS process, which showed that the performance of the CMOS SPAD detector was comparable to the performance of a conventional APD. Less than one molecule per detection volume element measured within 20 s gave a fitting standard errors of 1.2 and 5% for N and τ_D , which is certainly sufficient for most FCS measurements. The electronic performance of CMOS SPAD is very similar to that of conventional APDs: the detector exhibited no afterpulsing, a low dark count rate (40 Hz), and a short dead time (30 ns), but the detection efficiency of the detector is a factor of 10 lower than for a conventional APD with single-photon sensitivity. Next, the fraction of biomolecules (primer) in solution was determined with the CMOS SPAD. The results were clearly com-

parable with the results obtained with the SPCM APD, indicating that, apart from the lower detection efficiency, the CMOS SPAD can be used equally well for biomolecular analysis where different mobility distinguishes the actual content of a sample (e.g., binding interactions and enzymatic degradation). Finally, we showed the usefulness of the CMOS SPAD array for parallel FCS measurements with DOE multifocus illumination, wherein single biomolecular sensitivity was achieved in all four foci simultaneously. Unlike the former 2×2 array detection approach,¹⁴ the single spots could not be adjusted separately, which obviously results, for instance, in a lower count rate per molecule. However, despite lower count rates per molecule and high dark count rates in one of the detectors, equal sample concentrations were obtained when the effective detection volumes for the four detectors were calibrated individually.

We showed that a first step toward an integrated parallel single molecule detection system has been taken. To broaden its application and to make this kind of detector more powerful for biological and chemical applications at low concentrations, a higher detection efficiency and a larger active area of the detector are required and the detector sensitivity should be shifted to the red region as well. Low manufacturing costs, full integration of multiple Geiger-mode photodetector cells into smart detector arrays,¹⁸ and on-chip signal processing will lead to faster analysis and a smaller instrument, because analysis circuits (e.g., correlators) and software can become obsolete. Furthermore, novel and faster parallel single-molecule detection concepts for applications such as high throughput screening (HTS) and single molecule detection at low concentrations with huge data collection and data processing capacity (e.g., for screening and sequencing) might become feasible and inexpensive compared to parallel detection based on commercially available APD detectors.

Acknowledgments

This research was sponsored by the Commission for Technology and Innovation (CTI) of Switzerland and Gnothis S. A., Lausanne, Switzerland under Grant No. CTI 5814.1_sus. We would like to thank Holger Winter for important discussions in biochemistry, Per Thyberg for data analysis related questions, Mathias Johansson for the 2×2 DOE, Olympus Optical Ltd., Japan, for the diode-pumped solid state laser, and Mona Wells for her valuable comments on the manuscript. Gnothis SA is acknowledged for loaning equipment and the supply of biological samples.

References

1. R. Rigler and E. S. Elson, "Fluorescence Correlation Spectroscopy, Theory and Applications," F. P. Schäfer, W. Zinth and J. P. Toennies, Eds.; Springer-Verlag, Berlin, Heidelberg, New York (2001).
2. E. L. Elson and D. Magde, "Fluorescence correlation spectroscopy I: conceptual basis and theory," *Biopolymers* **13**, 1–27 (1974).
3. D. Magde, E. Elson, and W. W. W., "Fluorescence correlation spectroscopy II: an experimental realization," *Biopolymers* **4**, 29–61 (1974).
4. D. Magde, W. W. Webb, and E. Elson, "Fluorescence correlation spectroscopy. III. Uniform translation and laminar flow," *Biopolymers* **17**, 361–376 (1978).
5. R. Rigler, U. Mets, J. Widengren, and P. Kask, "Fluorescence correlation spectroscopy with high count rate and low-background—analysis of translational diffusion," *Eur. Biophys. J.* **22**, 169–175 (1993).
6. S. Wennmalm, L. Edman, and R. Rigler, "Conformational fluctuations in single DNA molecules," *Proc. Natl. Acad. Sci. U.S.A.* **94**, 10641–10646 (1997).
7. L. Edman, U. Mets, and R. Rigler, "Conformational transitions monitored for single molecules in solution," *Proc. Natl. Acad. Sci. U.S.A.* **93**, 6710–6715 (1996).
8. J. Widengren and R. Rigler, "Review—fluorescence correlation spectroscopy as a tool to investigate chemical reactions in solutions and on cell surfaces," *Cell Mol. Biol. (Oxford)* **44**, 857–879 (1998).
9. R. Rigler, A. Pramanik, P. Jonasson, G. Kratz, O. T. Jansson, P. A. Nygren, S. Stahl, K. Ekberg, B. L. Johansson, S. Uhlen, M. Uhlen, H. Jornvall, and J. Wahren, "Specific binding of proinsulin C-peptide to human cell membranes," *Proc. Natl. Acad. Sci. U.S.A.* **96**, 13318–13323 (1999).
10. J. Widengren, P. Schwillie, and R. Rigler, "Photophysical characterization of the dye Cy-5 by fluorescence correlation spectroscopy," *Biophys. J.* **72**, TU419–TU419 (1997).
11. M. Gösch, H. Blom, J. Holm, T. Heino, and R. Rigler, "Hydrodynamic flow profiling in microchannel structures by single molecule fluorescence correlation spectroscopy," *Anal. Chem.* **72**, 3260–3265 (2000).
12. M. Eigen and R. Rigler, "Sorting single molecules—application to diagnostics and evolutionary biotechnology," *Proc. Natl. Acad. Sci. U.S.A.* **91**, 5740–5747 (1994).
13. M. Auer, K. J. Moore, F. J. Meyer-Almes, R. Guenther, A. J. Pope, and K. A. Stoekli, "Fluorescence correlation spectroscopy: lead discovery by miniaturized HTS," *Drug Discov. Today* **3**, 457–465 (1998).
14. H. Blom, M. Johansson, A. S. Hedman, L. Lundberg, A. Hanning, S. Hard, and R. Rigler, "Parallel fluorescence detection of single biomolecules in microarrays by a diffractive-optical-designed 2×2 fan-out element," *Appl. Opt.* **41**, 3336–3342 (2002).
15. A. Koltermann, U. Ketting, J. Bieschke, T. Winkler, and M. Eigen, "Rapid assay processing by integration of dual-color fluorescence cross-correlation spectroscopy: high throughput screening for enzyme activity," *Proc. Natl. Acad. Sci. U.S.A.* **95**, 1421–1426 (1998).
16. H. Blom, M. Johansson, M. Gösch, T. Sigmundsson, J. Holm, S. Hard, and R. Rigler, "Parallel flow measurements in microstructures by use of a multifocal 4×1 diffractive optical fan-out element," *Appl. Opt.* **41**, 6614–6620 (2002).
17. A. Rochas, G. Ribordy, B. Furrer, P. A. Besse, and R. S. Popovic, "First passively-quenched single photon counting avalanche photodiode element integrated in a conventional CMOS process with 32ns dead time," *Proc. SPIE* **4833**, 107–115 (2003).
18. A. Rochas, M. Gösch, A. Serov, P. A. Besse, R. S. Popovic, T. Lasser, and R. Rigler, "First fully integrated 2D-array of single photon detectors in standard CMOS technology," *IEEE Photonics Technol. Lett.* **15**, 963–965 (2003).
19. M. Ehrenberg and R. Rigler, "Rotational Brownian motion and fluorescence intensity fluctuations," *Chem. Phys.* **4**, 390–401 (1974).
20. O. Krichevsky and G. Bonnet, "Fluorescence correlation spectroscopy: the technique and its applications," *Rep. Prog. Phys.* **65**, 251–297 (2002).
21. B. Rauer, E. Neumann, J. Widengren, and R. Rigler, "Fluorescence correlation spectrometry of the interaction kinetics of tetramethylrhodamin alpha-bungarotoxin with Torpedo California acetylcholine receptor," *Biophys. Chem.* **58**, 3–12 (1996).
22. M. Johansson, "Application and Design Developments in Diffractive Optics," in *Department of Microelectronics, Photonics Laboratory, School of Electrical and Computer Engineering*, p. 70, Chalmers University of Technology, Göteborg, Sweden (2001).
23. D. E. Koppel, "Statistical accuracy in fluorescence correlation spectroscopy," *Phys. Rev. A* **10**, 1938–1945 (1974).
24. T. Wohland, R. Rigler, and H. Vogel, "The standard deviation in fluorescence correlation spectroscopy," *Biophys. J.* **80**, 2987–2999 (2001).
25. U. Meseth, T. Wohland, R. Rigler, and H. Vogel, "Resolution of fluorescence correlation measurements," *Biophys. J.* **76**, 1619–1631 (1999).
26. P. Kask, R. Gunther, and P. Axhausen, "Statistical accuracy in fluo-

- rescence fluctuation experiments," *Eur. Biophys. J.* **25**, 163–169 (1997).
27. H. Qian, "On the statistics of fluorescence correlation spectroscopy," *Biophys. Chem.* **38**, 49–57 (1990).
28. M. Kinjo and R. Rigler, "Ultrasensitive hybridization analysis using fluorescence correlation spectroscopy," *Nucleic Acids Res.* **23**, 1795–1799 (1995).
29. N. L. Thompson, in *Fluorescence Correlation Spectroscopy*, Vol. 1: *Techniques*, J. R. Lakowicz, Ed., pp. 337–374, Plenum Press, New York (1991).